Universität Bremen

Fachbereich 4
Produktionstechnik
Maschinenbau &
Verfahrenstechnik

Advanced CERAMICS

Prof. Dr.-Ing.
Kurosch Rezwan
Fachgebiet
Keramische Werkstoffe
und Bauteile

IW 3, Raum 2131
Am Biologischen Garten 2
28359 Bremen

Tel. (0421) 218 - 64930
Fax (0421) 218 - 64932
E-Mail krezwan@uni-bremen.de
www www.ceramics.uni-bremen.de

Ansprechperson:
Dr.-Ing. Kamen Tushtev
E-Mail tushtev@uni-bremen.de
Tel. (0421) 218 – 64947

Datum: 15.11.18

University of Bremen, Advanced Ceramics
Am Biologischen Garten 2 / IW3, 28359 Bremen

Contact

J. Horvath, Dr.-Ing. K. Tushtev
E-Mail: tushtev@uni-bremen.de, Tel.: +49 421 218 64947

Customer

Walter Pritzkow
Walter E. C. Pritzkow Spezialkeramik
Adam Opel Str. 6
70794 Filderstadt (Sielmingen)

Instruction

Quite often, in tensile tests on dog-bone samples of fiber-reinforced CMC materials in 0/90 ° direction, the fracture (failure) occurs in the transition radius between the calibrated and the clamping region. In this study, the influence of the radius on the tensile strength was investigated. Another question was whether a narrower width in the clamping area could save material during sample preparation.

Samples

For the investigation, dog-bone samples as shown in Figure 1 were made of the material FW12 from Pritzkow Spezialkeramik. FW12 is a composite composed of a DF 11 fiber fabric (0/90° Nextel 610/1500 denier) from 3M and a matrix with a composition 85% Al_2O_3/15% 3YSZ.

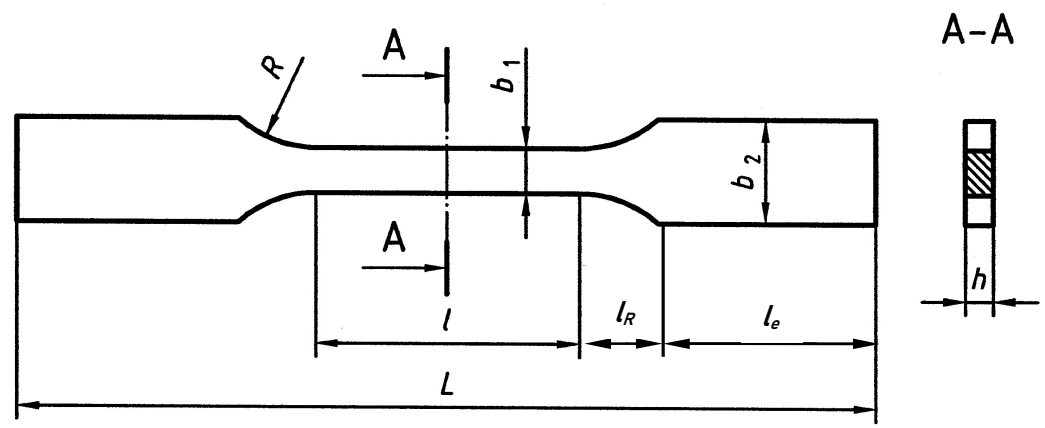

Fig. 1: Dog-bone specimens according to DIN EN 1893.

Experimental set-up

The dog-bone tensile specimens were manufactured with different radii *R* and different widths b_2 of the clamping area. The radii were 35, 50, 70, 100 and 140 mm. The clamping widths were 15 and 20 mm. For all samples, the calibrated length *l* remained constant at 40 mm, the sample width b_1 in the calibrated length remained 10 mm, the sample thickness *h* at 3 mm and the length in the clamping area l_e at 45 mm. The variations in the radius *R* and the clamping width b_2 gave different radii lengths l_R and overall lengths *L*. The specimen dimensions are summarized in Table 1. Three samples per each variant were tested.

Table 1: Sample sizes

Sample ID	Width b_2 mm	Radius R mm	Thickness h mm	Width b_1 mm	Overall length L mm
10_15_35	15	35	3	10	156
10_15_50	15	50	3	10	161
10_15_70	15	70	3	10	167
10_15_100	15	100	3	10	174
10_15_140	15	140	3	10	183
10_20_35	20	35	3	10	166
10_20_50	20	50	3	10	174
10_20_70	20	70	3	10	182
10_20_100	20	100	3	10	192
10_20_140	20	140	3	10	204

All tests were done on an universal testing machine Zwick Kappa 50 DS. Displacement-controlled tests were performed with 0.5 mm/min. The samples were clamped with sandpaper. The strain was measured by a laser extensometer with a reference length of L_0 = 25mm.

Notations and symbols according to DIN CEN/TR 13233

Overall length *L*, length of the sample in total, in mm

Calibrated length *l*, area of the sample with consistently smallest cross-sectional area, in mm,
(≥ 40mm according to DIN EN 658-1)

Reference length L_0, initial distance between the measuring marks on the sample within the calibrated length, in mm

Width b1, width of the sample within the calibrated length, in mm,
(≥ 8 mm according to DIN EN 658-1)

Width b2, (width of the sample within the clamped length) width at the end of the sample, in mm,
(b2 = a*b1, a = 1,2 till 2 according to DIN EN 1892/3 and 15157/8,
b2 ≥ 10mm according to DIN EN 658-1)

Thickness *h*, thickness of the sample within the calibrated length, in mm

Radius R or r, in mm
(> 30mm according to DIN EN 1892/3 und 15158, ≥ 30mm according to DIN EN 658-1)

Notations and symbols not according to DIN

Length of the sample ends l_e with width b_2 in mm.

Length in the transition radius (radius length) l_R in mm.

Experimental results

With one exception, all samples failed either in the transition radius or in the calibrated length. Representative photos are shown in Figure 2 and Figure 3.

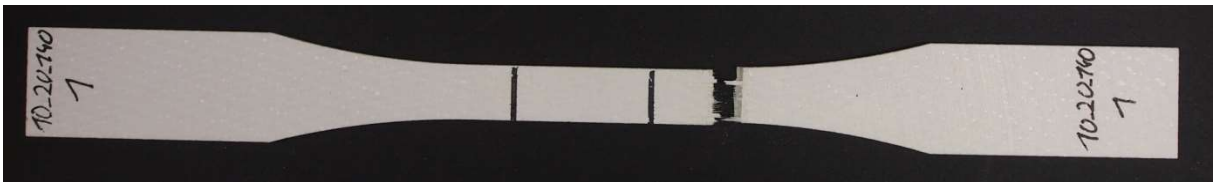

Fig. 2: Fracture type A for samples with a large transition radius.

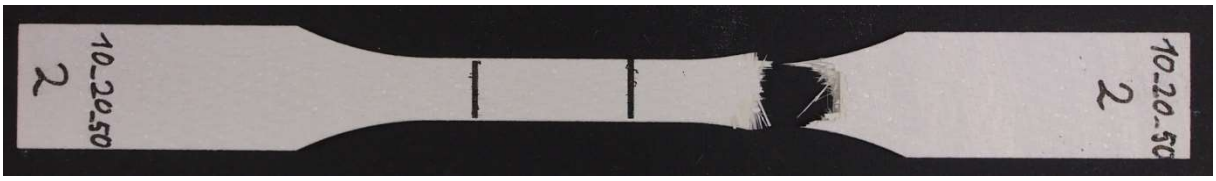

Fig. 3: Fracture type B for samples with a small transition radius.

The large radius samples failed in the calibrated length or in the transition region. The fracture is, as shown in Figure 2, smooth with small frays, Type A.

The samples with small radii failed mainly in the radius and show a largely smooth break in the middle of the sample with small fraying. At the edges, where the cross-section extends beyond b1 into the radius, long fraying occurs, since no load is transmitted here (shear failure), Figure 3, type B.

A sample with the designation 10_15_50 was broken in the clamping. Presumably the sandpaper had slipped between the clamping grips and thus the sample was only partially clamped.

Single values as well as mean values and standard deviations for the strengths, the E-Modules and the fracture positions are shown in Table 2 and Table 3.

Table 2: Single values of strength, E-modulus, position of fracture, and failure type.

Sample ID	Width b_2 mm	Radius mm	Strength MPa	E-Modulus GPa	Fracture distance l_a mm	Fracture width b_a mm	Fracture type
10_15_35_1	15	35	263	100	4,0	10,5	A
10_15_35_2			264	96	8,0	11,9	B
10_15_35_3			256	107	4,5	10,6	B
10_15_50_1	15	50	Break in the clamping				
10_15_50_2			266	94	6,5	10,8	B
10_15_50_3			267	105	10,5	12,2	B
10_15_70_1	15	70	263	108	9,5	11,3	B
10_15_70_2			274	112	10,5	11,6	B
10_15_70_3			267	93	7,5	10,8	B
10_15_100_1	15	100	265	99	10,0	11,0	A
10_15_100_2			265	96	13,0	11,7	B
10_15_100_3			275	105	7,0	10,5	A
10_15_140_1	15	140	282	96	8,5	10,5	A
10_15_140_2			284	99	7,5	10,4	B
10_15_140_3			283	97	1,5	10,0	A
10_20_35_1	20	35	267	103	0,0	10,0	A
10_20_35_2			264	93	10,0	12,9	B
10_20_35_3			261	93	10,0	12,9	B
10_20_50_1	20	50	271	100	8,0	11,3	B
10_20_50_2			267	99	10,0	12,0	B
10_20_50_3			267	102	10,0	12,0	B
10_20_70_1	20	70	281	101	7,0	10,7	B
10_20_70_2			286	91	4,0	10,2	A
10_20_70_3			276	124	12,0	12,1	B
10_20_100_1	20	100	275	92	0,0	10,0	A
10_20_100_2			290	113	10,0	11,0	B
10_20_100_3			269	103	8,0	10,6	B
10_20_140_1	20	140	286	108	2,0	10,0	A
10_20_140_2			287	99	2,0	10,0	A
10_20_140_3			291	99	0,0	10,0	A

Table 3: Averages of strengths, E-modules, and positions of fractures.

Sample ID	Width b_2 mm	Radius mm	Strength MPa	sd MPa	E-Modulus GPa	sd GPa	Fracture distance l_a mm	Fracture width b_a mm
10_15_35	15	35	261	4	101	5	5,5	11,0
10_15_50	15	50	266	1	100	5	8,5	11,5
10_15_70	15	70	268	5	105	8	9,2	11,2
10_15_100	15	100	269	4	100	4	10,0	11,1
10_15_140	15	140	283	1	97	1	5,8	10,3
10_20_35	20	35	264	3	96	5	6,7	11,9
10_20_50	20	50	268	2	100	1	9,3	11,8
10_20_70	20	70	281	4	105	14	7,7	11,0
10_20_100	20	100	278	9	103	8	6,0	10,5
10_20_140	20	140	288	2	102	4	1,3	10,0

Mean values and standard deviations of the strength and the E-modulus are shown graphically in diagrams 1 and 2.

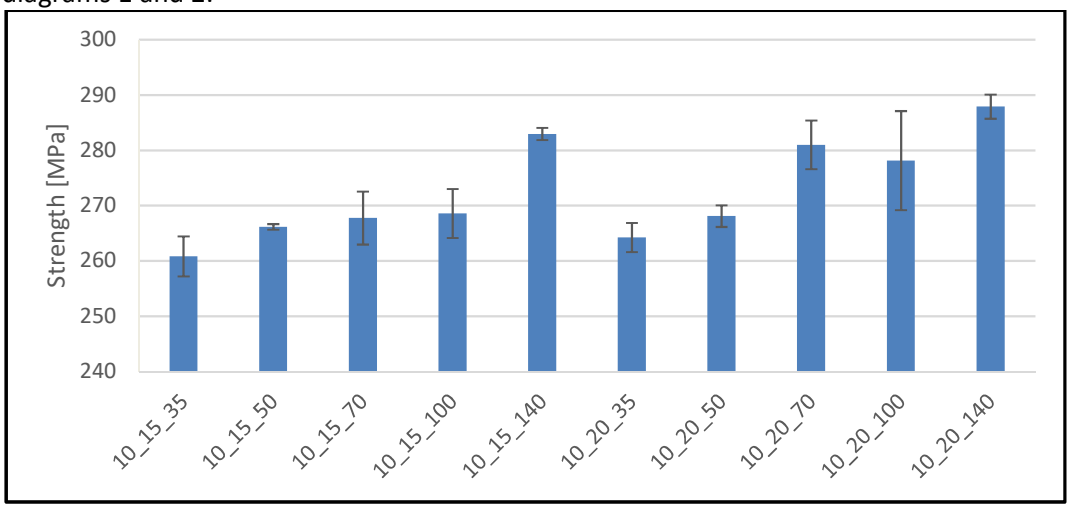

Diagram 1: Mean values and standard deviations of the strength.

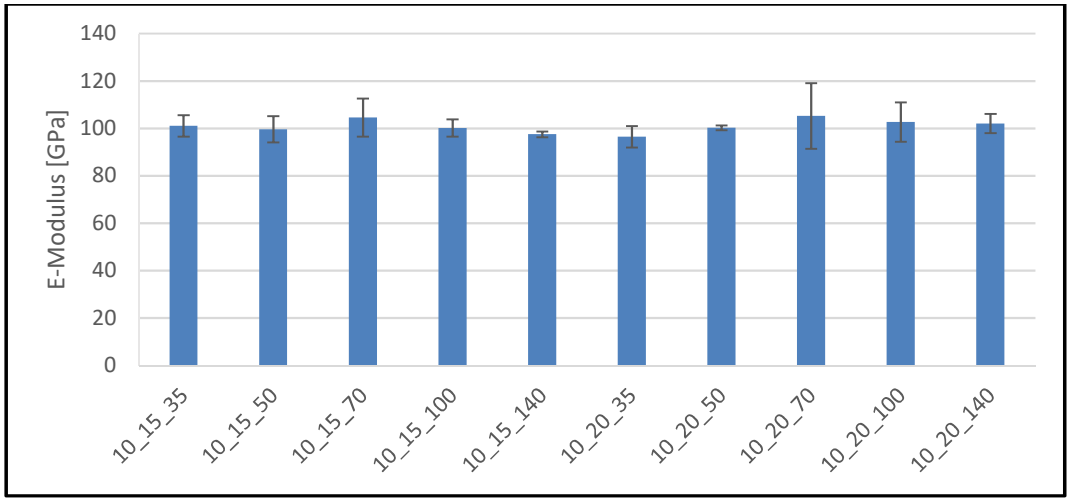

Diagram 1: Mean values and standard deviations of the E-modulus.

The mean modulus over all variations is 101 GPa +/- 3 GPa.

Strength

The measured strength over the different sample radii for both clamping widths 15 and 20 mm are shown below.

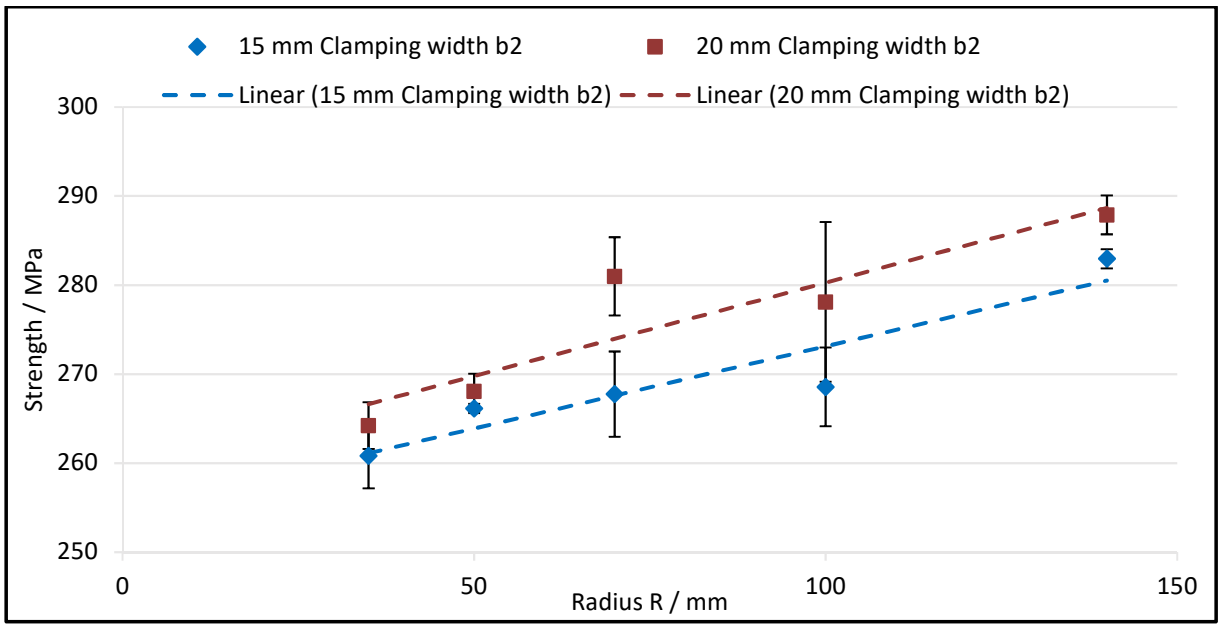

Diagram 2: Strength vs. radius R.

The trend is that the strength increases with larger radii. The increase over all radii is 22 MPa at 15mm clamping width and 24 MPa at 20mm clamping width, on average 23 MPa.

For the samples with a clamping width of 20 mm, the strength is on average 7 MPa higher than those with a clamping width of 15 mm.

Evaluation of fracture position

In addition to the strength and the E-modulus, the position of the fracture distance l_a and the fracture width b_a were measured, Figure 4. Most fractures occurred in the radius *R* and not in the calibrated length *l*. This changed only for the samples with large radii and 20 mm clamping width.

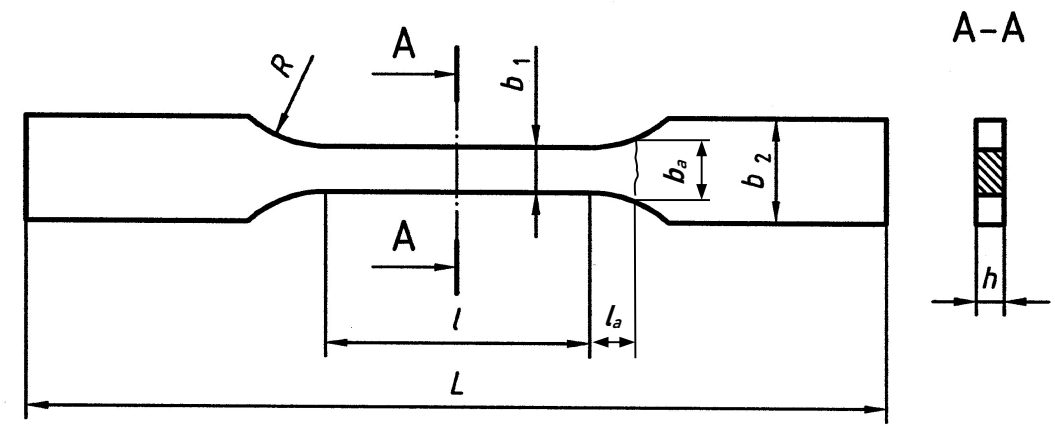

Fig. 4 : Distance l_a and width b_a for determination of the fracture position.

Additional Notation and Symbols:

Fracture position: fracture at the position l_a with width b_a.

Fracture distance l_a, distance of break from transition calibrated length in radius, mm

Fracture width b_a, sample width at break in radius at l_a, mm

If a break occurred in the calibration length l, the fracture distance l_a was set equal to 0 mm and the fracture width b_a as b_1.

Fracture distance l_a

Since the sample length of the radius l_R depends on the size of the radius, the distance of the fracture to the calibrated length for small radii cannot be as long as the same distance for the large radii. For this reason, the fracture distance l_a was related to the radius length l_R and a relative fracture distance l_a/l_R was calculated. Diagram 4 shows the mean values and standard deviations.

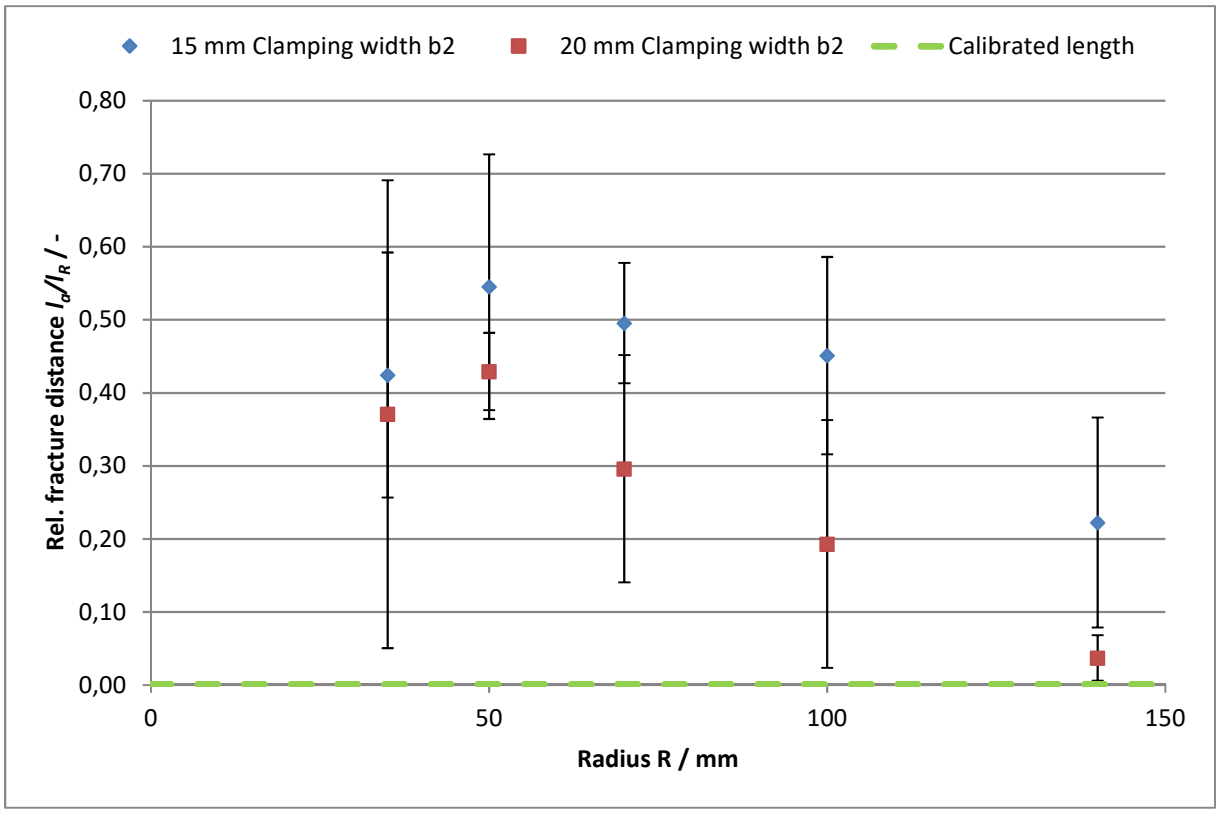

Diagram 3: Relative fracture distance l_a/l_R vs. radius *R*.

As the radius increases, the relative fracture distance becomes smaller. For large sample radii, the fracture will be either closer to the calibrated length or within the calibrated length.

All samples with a 20 mm clamping width break at a shorter relative breaking distance than with a 15 mm clamping width.

Sample width at Fracture b_a

The fracture width b_a was also related to the sample width b_1. Diagram 5 shows the mean relative fracture width b_a/b_1 and their standard deviation.

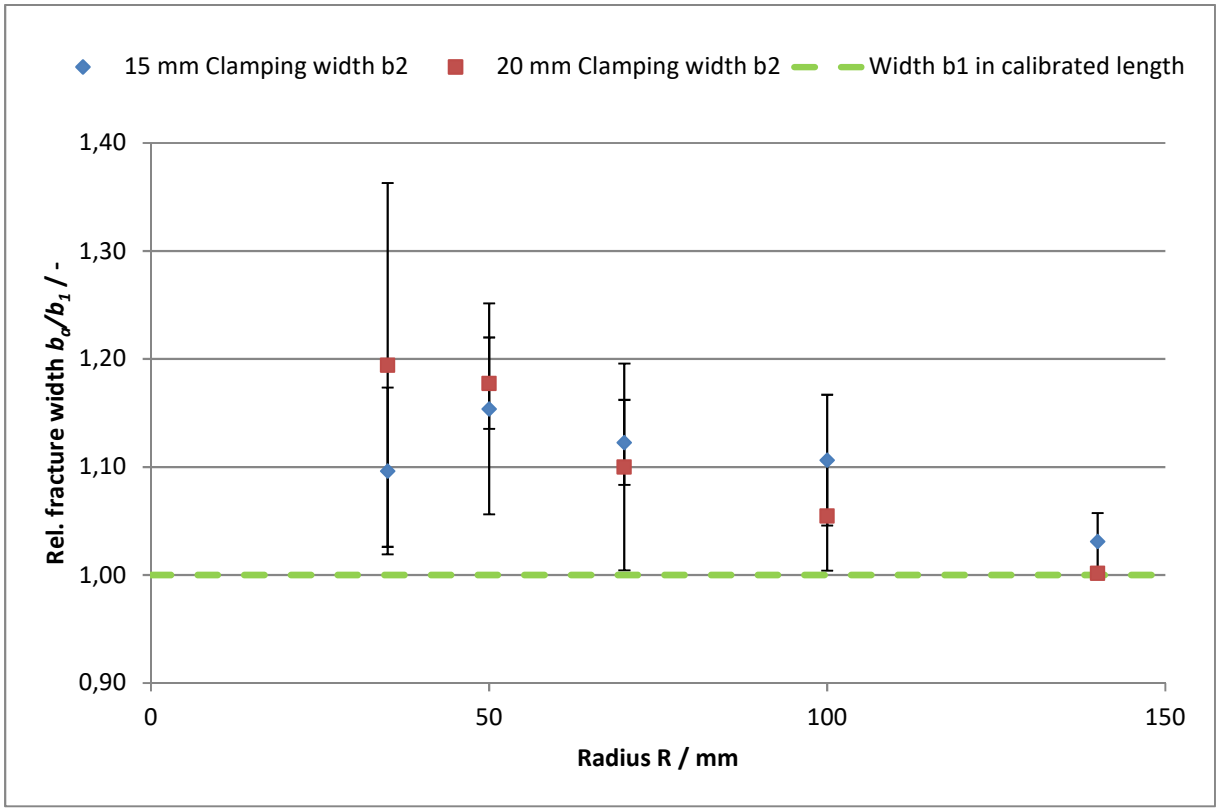

Diagram 4: Relative fracture width b_a/b_1 vs. radius *R*.

The relative fracture width decreases with increasing radius R. In other words, the fracture width b_a approaches or corresponds to the sample width b_1 as the radius increases.

Bremen, 15.11.2018

Dr.-Ing. Kamen Tushtev